International Journal of Naval Architecture and Ocean Engineering 13 (2021) 566–574

Contents lists available at ScienceDirect

International Journal of Naval Architecture and Ocean Engineering

journal homepage: http://www.journals.elsevier.com/international-journal-of-naval-architecture-and-ocean-engineering/

A new cavitation model considering inter-bubble action

Yazhen Shi [a], Kai Luo [a], Xiaopeng Chen [a, *], Daijin Li [a], Laibing Jia [b]

[a] School of Marine Science and Technology, Northwestern Polytechnical University, Xi'an, PR China
[b] Department of Naval Architecture Ocean and Marine Engineering, University of Strathclyde, Glasgow, United Kingdom

ARTICLE INFO

Article history:
Received 22 April 2021
Received in revised form
26 May 2021
Accepted 29 May 2021
Available online 8 June 2021

Keywords:
Bubble–bubble interaction
Bubble cloud
Cavitation model

ABSTRACT

The process of cavitation involves generation, growth, coalescence, and collapse of small bubbles and is tremendously influenced by bubble–bubble interactions. To understand these interactions, a new cavitation model based on the transport equation is proposed herein. The modified Rayleigh–Plesset equation is analyzed to determine the bubble growth rate by assuming equal-sized spherical bubble clouds. The source term in the transport equation is then derived according to the bubble growth rate with the bubble-bubble interaction. The proposed model is validated by various test simulations, including microscopic bubble cloud evolution as well as macroscopical two- and three-dimensional cavitating flows. Compared with previous models, namely the Kunz and Zwart cavitation models, the newly proposed model does not require adjustable parameters and generally results in better predictions both microscopic and macroscopical cases. This model is more physical.

1. Introduction

Cavitation is a phenomenon involving the sudden transition in the state of matter from liquid to vapor induced by decreasing local pressures below the vapor pressure (Chen, 2010). It is an undesirable process in many circumstances that degrades the performance of hydraulic machinery and reduces the efficiency of hydroturbines (Wang et al., 2020). Some other drawbacks, such as noise emission, vibration, and surface erosion, are also associated with cavitation (Peng et al., 2017). However, cavitation has been applied to surface cleaning and drug delivery techniques (Gevari et al., 2020; Stride et al., 2020).

Inter-bubble action plays an essential role in cavitation. In practice, cavitation begins with the explosive growth of gas nuclei to visible bubbles; these bubbles then grow, coalesce, and collapse while interacting with each other. Mettin et al. (1993) studied the interaction forces between two small coupled bubbles in an acoustic field, where the secondary Bjerknes forces were also considered. Ida (2009) found suppression of cavitation inception due to interaction: the cavitation threshold pressure of a small bubble decreases under the action of a nearby bubble. Bremond et al. (2006) explored the collapse and expansion of arrayed bubbles confined on a patterned plate. The evolution of these bubbles was described using the extended Rayleigh–Plesset (R–P) equation, with the bubble interactions.

Numerical simulations are useful tools for exploring the dynamics of bubble clusters. On a microscopic level, numerical simulations resolve the flow details well, including bubble–bubble interactions. Ma et al. (2018) studied a bubble cloud exposed to a sinusoidal pressure field using the Eulerian–Lagrangian approach. The nonlinearity in the dynamics was explored with various excitations. The influences from bubble–wall distance and bubble–bubble spacing were investigated by Zhang et al. (2019) in a 27-bubble cloud. The collapse sequence and impulsive pressure were observed to depend strongly on the geometry of the cloud. Tiwari et al. (2015) simulated the expansion and collapse of a cluster of 50 bubbles; the study showed that bubble–bubble interactions were profound and had great impacts on the peak pressure, bubble volume, and shape evolution. Meanwhile, Direct Numerical Simulation (DNS) incurs extremely heavy computational loads (Rasthofer et al., 2019), which renders it unrealizable for large-scale cavitating flow simulations.

On a macroscopic level, the dynamics of cavitation bubble clusters are studied using models. The balance between accuracy and computational efficiency is also carefully considered in the modeling. In this regard, the "homogeneous equilibrium" models have achieved great success (Roohi et al., 2013); in these models, the mixture of liquid and vapor/bubble phases is described as a single fluid whose properties depend on the contents of the

* Corresponding author.
E-mail address: xchen76@nwpu.edu.cn (X. Chen).
Peer review under responsibility of The Society of Naval Architects of Korea.

https://doi.org/10.1016/j.ijnaoe.2021.05.005

mixture. Two types of models are thus identified to obtain the density distribution of the mixture. The first type is the Barotropic Equation Model (BEM), where a special Equation of State (EOS) is prescribed for the pressure-specific volume relation of the mixture (Delannoy and Kueny, 1990; Goncalves and Patella, 2009); it was developed to simulate shocked flows in the presence of cavitation in cryogenic liquids, and the accuracy of simulation depends strongly on the choice of the EOS. The second type is based on the Transport Equation Model (TEM), where the phase transition is modeled in the transport equation; the mass source term in the equation is solved by a simplified R–P equation (Sauer and Schnerr, 2001; Singhal et al., 2002; Zwart et al., 2004), and this type of model is used in various simulations because of its lower computational loads and accurate results.

Although large numbers of bubbles exist in cavitation flows (Wan et al., 2017), with the inter-bubble actions known to be pronounced in bubble dynamics (Ida, 2009; Bremond et al., 2006; Zhang et al., 2016; Maeda and Colonius, 2018), the interactions are ignored in most traditional cavitation models, including many TEMs. Only a few relevant works have considered the details of the bubble cluster. Du et al. (2016) proposed a modified full cavitation model, which considered the bubble size distribution and breakup effects; they found that the internal structure of the cavitation cloud influenced its collapse, while ignoring the bubble–bubble interactions that caused the lower collapse pressure. Ye et al. (2016) considered the second-order derivative and bubble–bubble interaction in their cavitation model. Furtherly, they proposed a model that generated better predictions than the traditional Zwart-Gerber-Belmri (ZGB) cavitation model (Zwart et al., 2004). In their study, Ye et al. modified some parameters in the equation artificially to achieve the bubble growth rate. Maiga et al. (2018, 2019) derived a new model based on the mutual interactions between two spherical bubbles with different sizes, and the only input was the local velocity divergence; the effectiveness of this model was validated. However, the local velocity divergence must be obtained before the predictions, which limits the model's application.

In the present study, a new cavitation model based on the TEM is derived from the modified R–P equation coupled with inter-bubble actions (Bremond et al., 2006). The second-order derivative and surface tension are also considered here. Compared with Ye's model (Ye et al., 2016), the present model is directly derived from the modified R–P equation and is more concise. The remainder of this paper is organized as follows. In Section 2, a new cavitation model is derived with appropriate assumptions. In Section 3, the bubble cluster evolutions in cavitation flow around a two-dimensional hydrofoil and three-dimensional flow around a cylinder with a spherical head are simulated using the proposed model. In Section 4, the conclusions of the study are presented.

2. Proposed cavitation model

2.1. Estimation of bubble growth

In the present study, the inter-bubble actions are considered for cavitation in the TEM, where the classical R–P equation is considered as the basis for describing bubble dynamics (Plesset, 1949):

$$R^2\ddot{R}+\frac{3}{2}\dot{R}^2=\frac{1}{\rho_l}\left(p_v-p-\frac{4\mu\dot{R}}{R}-\frac{2S}{R}\right). \tag{1}$$

In the equation, R is the time-dependent bubble radius, and the over-dots represent the time derivatives; ρ_l, μ, and S are the liquid density, viscosity, and interfacial tension, respectively; p_v and p are the vapor pressure and ambient pressure, respectively. The left-hand-side of the equation represents the inertia of the liquid, and the right-hand-side represents the driving force. Neglecting the second-order derivative and the influences of viscosity and surface tension (Plesset, 1949; Brennen, 1993), the equation can be recast as

$$\dot{R}=sign(p_v-p)\sqrt{\frac{2}{3}\frac{|p_v-p|}{\rho_l}}, \tag{2}$$

which provides a simplified estimation of the bubble growth speed. This form has been applied as a basis in many previous models (Sauer and Schnerr, 2001; Singhal et al., 2002; Zwart et al., 2004).

As shown in the previous studies (Ida, 2009; Bremond et al., 2006), the inter-bubble action is associated with the pressure field induced by the neighboring bubble motion. The interactions cause the bubbles to evolve and move. The motions, growth, and deformations of the bubbles are coupled and time dependent, for which only numerical results have been obtained. To introduce the interactions without complicating the problem, we assume the following: (1) identical bubbles are distributed evenly in the cloud, (2) the relative positions of the bubbles are fixed during the cavitation process, (3) the bubbles are always spherical, and (4) the number of bubbles is constant (Kubota et al., 1992). The R–P equation is then modified as

$$R\ddot{R}+\frac{3}{2}\dot{R}^2=\frac{1}{\rho}\left(P_B-P_\infty-\frac{4\mu\dot{R}}{R}-\frac{2S}{R}\right)-\frac{d}{dt}\left(\sum\frac{R_i^2\dot{R}_i}{D_i}\right),\ (R_i\equiv R). \tag{3}$$

where the last term in the equation, i.e., $(R_i^2\dot{R}_i/D_i)$, denotes the pressure imposed on the target bubble induced by the i-th bubble of radius R_i; D_i is the distance from the i-th bubble to the target bubble, and the detailed derivation can be found in (Mettin et al., 1993). Noting that D_i is fixed and introducing the number density of the bubbles in space, n, we have

$$\sum_i\frac{1}{D_i}\approx\int_{l_{min}}^{l_{max}}\frac{4\pi nr^2}{r}dr=2\pi nl_{max}^2, \tag{4}$$

where l_{min} is the distance between a bubble and its nearest neighbor, and $l_{max}(\gg l_{min})$ is the truncated distance. Therefore, the last term in Eq. (3) can be rewritten as

$$\sum_i\frac{1}{D_i}\frac{d}{dt}\left(R_i^2\dot{R}_i\right)=\frac{d}{dt}\left(\dot{R}R^2\sum_i\frac{1}{D_i}\right)=2\pi l_{max}^2\left[nR^2\ddot{R}+2nR\dot{R}^2\right]. \tag{5}$$

Substituting Eq. (5) into Eq. (3) gives

$$R\ddot{R}+\frac{3}{2}\dot{R}^2+2\pi l_{max}^2\left(nR^2\ddot{R}+2nR\dot{R}^2\right)=\frac{1}{\rho}\left(p_v-p-\frac{4\mu\dot{R}}{R}-\frac{2S}{R}\right), \tag{6}$$

whose left-hand side can be simplified as

$$\frac{1}{2}\frac{1}{R^2\dot{R}}\frac{d}{dt}\left(R^3\dot{R}^2+2\pi nl_{max}^2R^4\dot{R}^2\right). \tag{7}$$

Then, Eq. (6) is recast as

$$\frac{d}{dt}\left(R^3\dot{R}^2+2\pi nl_{max}^2R^4\dot{R}^2\right)=\frac{2R^2\dot{R}}{\rho}\left(p_v-p-\frac{4\mu\dot{R}}{R}-\frac{2S}{R}\right). \tag{8}$$

Assuming $dp/dt = 0$ and $\mu = 0$, the right-hand side in Eq. (8) is simplified as

$$\frac{d}{dt}\left(\frac{2(p_v - p)}{3\rho}R^3 - \frac{2S}{\rho}R^2\right). \tag{9}$$

Combining Eqs. (8) and (9), the bubble growth rate is achieved as

$$\dot{R} = sign(p_v - p)\sqrt{\frac{\left|\frac{2(p_v-p)}{3\rho}\left[1-\left(\frac{R_0}{R}\right)^3\right] - \frac{2S}{\rho}\frac{(R^2-R_0^2)}{R^3}\right|}{1 + 2\pi n l_{max}^2 R}}. \tag{10}$$

Furthermore, the target bubble can be interacted by surrounding several layer bubbles. The truncated distance l_{max} can be obtain as $l_{max} = kn^{-1/3}$, in which k defines the number of surrounding interaction layer. We have

$$\dot{R} = sign(p_v - p)\sqrt{\frac{\left|\frac{2(p_v-p)}{3\rho}\left[1-\left(\frac{R_0}{R}\right)^3\right] - \frac{2S}{\rho}\frac{(R^2-R_0^2)}{R^3}\right|}{1 + 2\pi k^2 n^{1/3} R}}. \tag{11}$$

2.2. Modified mass transport equation

As mentioned before, the interactions between the bubbles are neglected in most cavitation models based on the Transport Equation (TE). In this work, the bubble growth rate is coupled with the mass transport equations of vapor and liquid. The mass transport equations for vapor and liquid are expressed as (Du et al., 2016)

$$\frac{\partial \alpha\rho_v}{\partial t} + \frac{\partial(\alpha\rho_v u_i)}{\partial x_i} = S_r, \tag{12}$$

$$\frac{\partial (1-\alpha)\rho_l}{\partial t} + \frac{\partial[(1-\alpha)\rho_l u_i]}{\partial x_i} = -S_r, \tag{13}$$

respectively, and the *Einstein notation* is used in these equations. The subscripts m, v, and l represent mixture, vapor, and liquid, respectively; α $(= 4n\pi R^3/3)$ is the volume fraction of the vapor phase; S_r is the source term describing the mass transported between two phases. The local density and viscosity of the mixture are linearly interpolated as

$$\rho_m = \alpha\rho_v + (1-\alpha)\rho_l, \tag{14}$$

$$\mu_m = \alpha\mu_v + (1-\alpha)\mu_l. \tag{15}$$

Summarizing Eqs. (12) and (13), the continuity equation for the mixture is obtained as

$$\frac{\partial \rho_m}{\partial t} + \frac{\partial(\rho_m u_i)}{\partial x_i} = 0. \tag{16}$$

On the other hand, taking Eq. (12)$\times\rho_l$ + Eq. (13)$\times$ ρ_v, the source term S_r can be derived as

$$S_r = \frac{\rho_l\rho_v}{\rho_l - \rho_v}\frac{\partial u_i}{\partial x_i} = -\frac{\rho_l\rho_v}{\rho_l - \rho_v}\frac{1}{\rho_m}\frac{D\rho_m}{Dt}. \tag{17}$$

Then, we take the derivative of Eq. (14) to obtain

$$\frac{D\rho_m}{Dt} = -(\rho_l - \rho_v)\frac{D\alpha}{Dt}, \tag{18}$$

and substitute it into Eq. (17) to get

$$S_r = \frac{\rho_l\rho_v}{\rho_m}\frac{D\alpha}{Dt} = \frac{3\alpha}{R}\frac{\rho_l\rho_v}{\rho_m}\dot{R}. \tag{19}$$

Combining Eqs. (11) and (19), the source term can be written as

$$S_r = sign(p_v - p)\frac{3\alpha}{R}\frac{\rho_l\rho_v}{\rho_m}\sqrt{\frac{\left|\frac{2(p_v-p)}{3\rho_m}\left[1-\left(\frac{R_0}{R}\right)^3\right] - \frac{2S}{\rho_m}\frac{(R^2-R_0^2)}{R^3}\right|}{1 + 2\pi k^2 n^{1/3} R}}, \tag{20}$$

where $R = \left(\frac{3}{4}\frac{\alpha}{n\pi}\right)^{1/3}$ and $R_0 = \left(\frac{3}{4}\frac{\alpha_0}{n\pi}\right)^{1/3}$. Based on the Schnerr and Sauer model (Sauer and Schnerr, 2001), the constants $n = 1.6 \times 10^{13}$ and $R_0 = 1.0 \times 10^{-6} m$ are adopted in the present work.

2.3. Numerical approach

The above model was embedded in an open-source package, OpenFOAM, where the general numerical approach depicted in Fig. 1 was used. In the approach, the unsteady Reynolds averaged Navier–Stokes (RANS) equations for the mixture were solved using

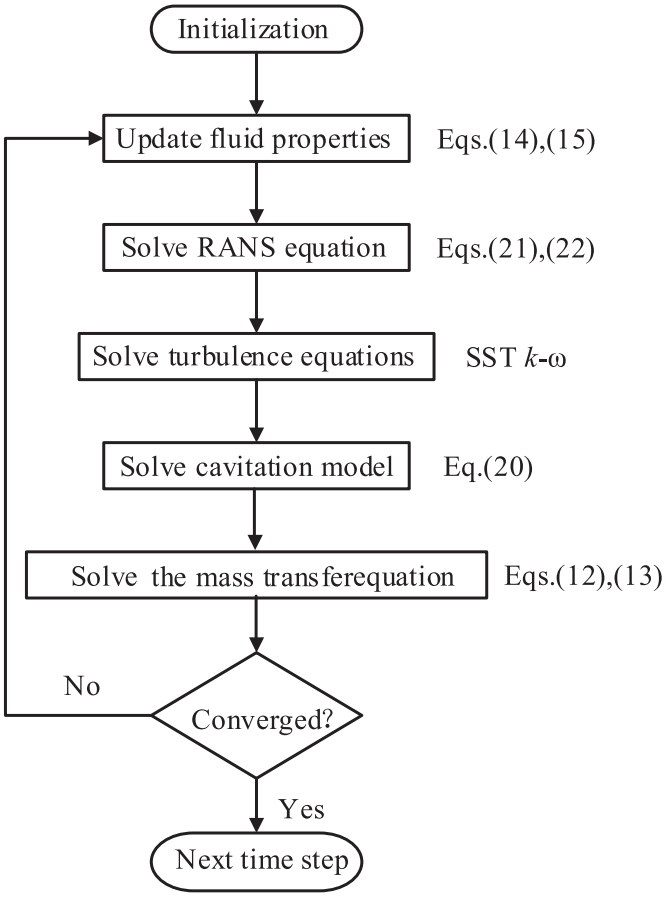

Fig. 1. Algorithm for the numerical approach.

the SIMPLE algorithm.

$$\frac{\partial \rho_m}{\partial t}+\frac{\partial\left(\rho_m u_j\right)}{\partial x_j}=0, \tag{21a}$$

$$\frac{\partial}{\partial t}\left(\rho_m u_i\right)+\frac{\partial\left(\rho_m u_i u_j\right)}{\partial x_j}=$$

$$-\frac{\partial p}{\partial x_i}+\frac{\partial}{\partial x_j}\left[\left(\mu_m+\mu_t\right)\left(\frac{\partial u_i}{\partial x_j}+\frac{\partial u_i}{\partial x_i}-\frac{2}{3}\frac{\partial u_k}{\partial x_k}\delta_{ij}\right)\right], \tag{21b}$$

In the equation, μ_m is the mixture's laminar viscosity and μ_t is the turbulent viscosity; μ_t is updated according to the Shear Stress Transport (SST) $k-\omega$ turbulence model (Menter, 1993). A second-order upwind and a second-order central difference scheme were used to handle the convection and diffusion terms in Eq. (21b), respectively. The local volume fraction of vapor was solved according to the newly derived TE, namely Eqs. (12) and (20), where the Volume of Fluid (VOF) method was used (Hirt and Nichols, 1981). These equations were compiled in OpenFOAM first before the simulation.

3. Results and discussion

The proposed model was tested for several cases and compared with the DNS and other well-developed cavitation models. The tests include cavitating bubble cluster evolution, cavitating flows around a two-dimensional Clark-Y hydrofoil, and a three-dimensional cylinder with a hemispherical head.

3.1. Collapse of a bubble cloud

Noting that cavitating flows have strong bubble dynamic fundamentals, the collapse of a bubble cloud can be approximated by DNS. The feasibility of Eq. (11) is first checked, and the numerical setup follows that of Zhang et al. (2019), as illustrated in Fig. 2. The bubble cloud in a cubic region initially consists of 64 spherical vapor bubbles with the same radii ($r = 4$ mm). The distance between the nearest neighboring bubbles is 12 mm, corresponding to the bubble number density $n = 5.8\times10^5(1/\mathrm{m}^3)$ and volume fraction $\alpha\approx0.2$. The cloud is located around the center of the computational domain of size $150\times150\times150\mathrm{mm}^3$. Initially, the vapor pressure, $p_v = 2300$ Pa, is set for each bubble, and a far-field boundary condition with a constant pressure $p_0 = 0.1$ MPa is imposed on all the sides. The bubbles collapse under the pressure difference, $\Delta p = p_0 - p_v$. In the calculations, an adjustable time step is applied to ensure that the CFL number is less than 0.3. A nonuniform Cartesian grid is adopted with the grid number of about 10^7; the grid is refined in the cluster region, and the diameter of the bubble is resolved using 35 cells.

Fig. 2 shows the evolution of the bubbles in the cluster, and Fig. 3 shows the corresponding transient total vapor volume (V_{Tot}) and bubble collapse rate ($\dot{R}$). The predictions of Eqs. (2) and (11) with $k = 1$, 2, and 3 are compared, which are solved using the Runge–Kutta method. The total vapor volume is thus obtained directly from the simulation, and the bubble collapse rate is calculated by taking the time derivative of the equivalent radius according to the total vapor volume: $R_{eqv}\sim V_{tot}^{1/3}/4^3$. A smaller value for k means weak interaction, and bubbles collapse without restraint. A lager value means strong interaction. The vapor volume and collapse rate deviate from the numerical curve both $k = 1$ and 3, and 2 is the optimal value for k, especially in initial collapse stage.

Although Fig. 2 shows that the bubbles collapse layer by layer from the outside to the inside, Eq. (11) adequately predicts the vapor volume variation qualitatively, especially for 0–0.5 ms. Eq. (2) provides poor predictions for both the total vapor volume and bubble collapse rate. Without considering the interactions, the collapse rate has a constant value, which is purely determined by Δp, leading to a $V_{Tot}\sim -t^3$ relation. This is the basis of the previous TEM (such as the Zwart model) and is inaccurate for predicting bubble cluster evolution.

With the present model, both the interaction and inertial effects are considered. The inertia effect is reflected by the R_0 terms in Eq. (11). Fig. 3 shows that the results from DNS and Eq. (11) indicate a slow start for the collapse, and the collapse rate accelerates gradually with time. It is seen that the results of the DNS and present model agree well with each other at the early stage ($t<0.5$ ms). Thereafter, a sudden increase in the collapse rate due to inertia is observed in both the DNS and theoretical predictions (Fig. 3(b)). Without considering the inertia and inter-bubble actions, Eq. (2) overestimates the collapse rate and predicts earlier disappearance of the bubbles. Evidently, one can see that the predicted collapse

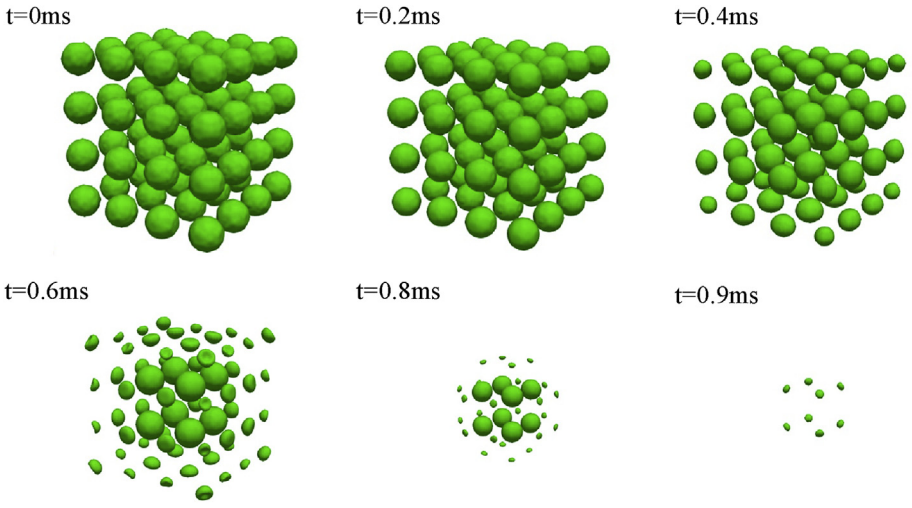

Fig. 2. Temporal evolution of the collapsing cloud (the top left image shows the initial state of the bubble cluster with $4\times4\times4$ bubbles and far-field pressure boundary conditions imposed on the sides of the computational domain).

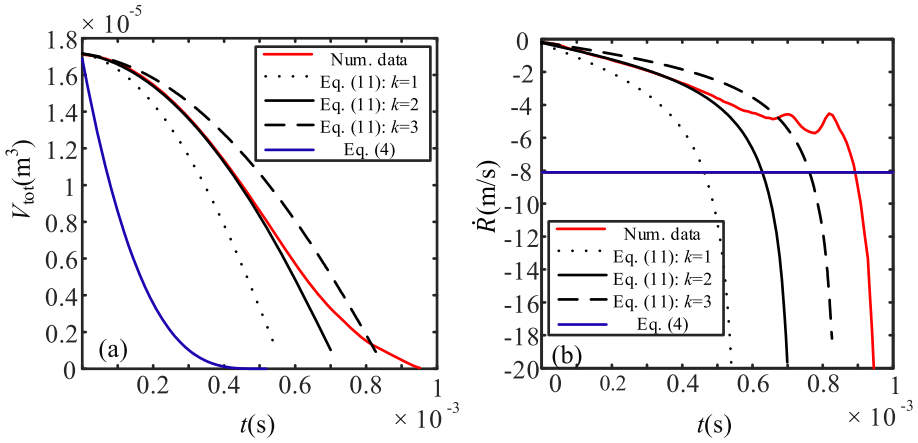

Fig. 3. Comparison of the numerical results with theoretical predictions from Eqs. (2) and (11). In Eq. (11), k = 1, 2, and 3 are adopted: (a) total vapor volume evolution; (b) average bubble collapses rate.

time by Eq. (11) is also shorter than that suggested by the DNS result. From Fig. 2, we note that the discrepancy manifests after t = 0.6 ms, when the bubbles in the outer layer show apparent deformation and are much smaller than those in the inner layer. They do not satisfy the assumptions (1) and (3) proposed in Section 2. However, the discrepancies only manifest at the late stage of collapse when V_{Tot} becomes small. This deviation causes errors of only 3.08% and 3.02% in ρ_m and μ_m, respectively, according to Eqs. (14) and (15), which can be generally neglected in cavitating flow simulations (see the next subsection). Hence, we use Eq. (11) in our model. According to Fig. 3, a modification on the cavitation model might remedy the problem of overestimation of the collapse of the cavity (Niederedzka et al., 2016).

The consistency between the results of the DNS and prediction of Eq. (11) allows a solid basis for further simulations. Considering the bubble interactions and the second-order derivative, the simulations provide better descriptions for bubble cluster dynamics.

3.2. Sheet/cloud cavitation on a two-dimensional hydrofoil

The TE model is applied to simulate cavitating flows for further validation with a two-dimensional Clark-Y hydrofoil. The numerical setup is as depicted in Fig. 4, and the flow conditions are according to literature (Wang et al., 2001; Huang et al., 2013). In the simulations, the chord length of the hydrofoil c = 7 cm and the angle of attack AOA = 8°; the no-slip boundary condition is imposed on the hydrofoil. The free-stream velocity, U_∞ = 10 m/s, is imposed at the inlet with a turbulent intensity of 2%. The outlet pressure p_o = 43269 Pa and the saturation pressure is p_v = 3269 Pa. The corresponding cavitation number and Reynolds number are $\sigma = \frac{(p_o - p_v)}{\rho_l U_\infty^2}$ = 0.8 and $Re = \rho_l c U_\infty / \mu_l = 7 \times 10^5$, respectively.

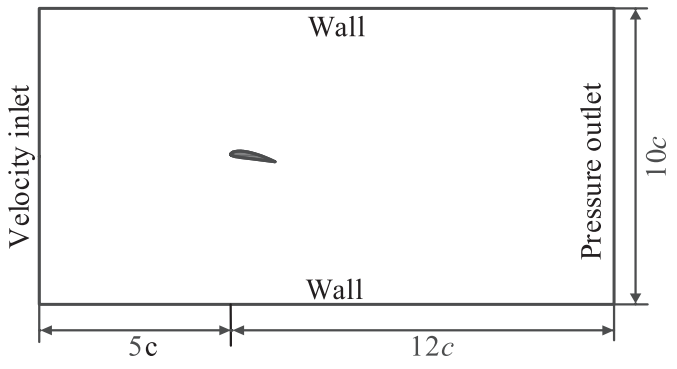

Fig. 4. Illustration of the computational domain for cavitating flow and boundary conditions.

With regard to the large Reynolds number applied, the SST $k-\omega$ turbulence model is adopted, which is appropriate in flow simulations with adverse pressure gradients (Menter, 1993) and is accurate for cavitating flow simulations (Goncalves, 2011). Meanwhile, 1.6×10^5 grids with $y^+ = 1-2$ (near the hydrofoil wall) and a time step of $\Delta t = 1 \times 10^{-6}\text{s} < T_{\text{ref}}/100 (T_{\text{ref}} = c/U_\infty)$ (Long et al., 2017) are adopted for accurate simulations. In Sections 3.2 and 3.3, we only replace the cavitation model in the comparisons, while the numerical setup and other parameters are identical.

The experiments show that the cavitating flow with the above flow condition is semi-periodic owing to the reattachment of the flows on the surface of the hydrofoil (Huang et al., 2013). The snapshots of the cavity developing in a cycle are shown in Fig. 5, where the experiments and numerical results obtained from the proposed and Kunz cavitation models are illustrated. Both numerical models capture the primary features of cavity development. The results show that cavitation occurs at the leading edge and grows until it covers most of the hydrofoil. Thereafter, a re-entrant jet appears, which travels backward to the leading edge resulting in shedding of the cavity from the foil surface. The cavity patterns from the proposed model are more similar to those of the experiments in the shedding stage.

From the numerical results, the time-averaged lift and drag coefficients,

$$C_L = \frac{Lift}{0.5\rho U_\infty Sc}, C_d = \frac{Drag}{0.5\rho U_\infty Sc}, \tag{22}$$

are estimated over eight cycles. The results from different sources are compared in Table 1, including experiments (Huang et al., 2013) and numerical results using the Kunz and proposed cavitation models. It can thus be seen that the present model improves the accuracy of the simulations.

Further comparisons are shown in Fig. 6, where the ensemble-averaged streamwise velocity (u) and flow structure are shown more clearly. The newly proposed model produces better results compared with the Kunz model. It is seen that near the leading edge ($x/c \approx 0.2$), the time-averaged u component is generally positive; in this region, the two models produce similar results, which agree with the experiments. However, the present model provides more accurate predictions in the rear part of the foil (x/c =

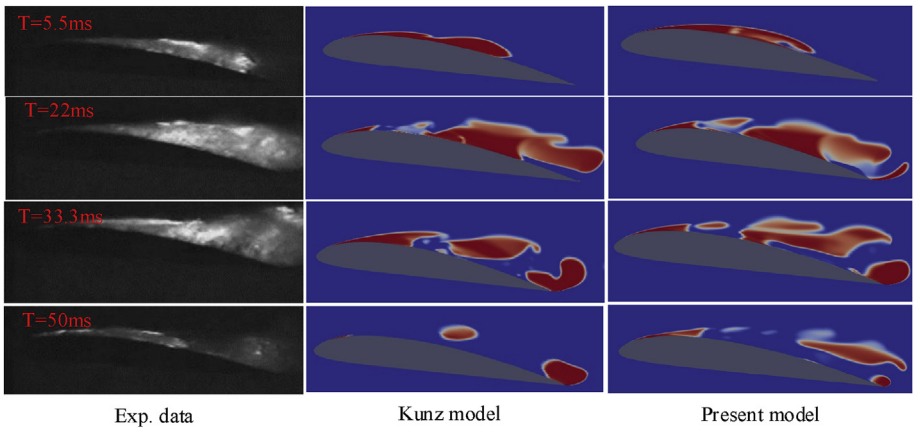

Fig. 5. Evolution of the cavities in a cycle. Left to right: experiments (Wang et al., 2001), numerical results from the Kunz cavitation model, and results from the proposed cavitation model.

Table 1
Averaged lift and drag coefficients for cloud cavitation.

Cavitation model	C_l	C_d
Experimental data	0.760	0.119
Kunz model	0.742	0.13
Proposed model	0.763	0.122

0.6, 0.8), where the negative u-component is found for the re-entrant jet. As shown in Fig. 5, the cavity sheds with a pronounced vortex motion in this region, which significantly influences the lift and drag. Again, the proposed cavitation model can capture the unsteady periodic behaviors of cloud cavitation accurately.

3.3. Cavitation around cylinder

Based on the presented tests, it is also noted that the traditional cavitation models, such as the Kunz and Zwart models, require adjustable parameters for accurate predictions; unfortunately, these values are significantly different from the present work to reported literature (see Table 2). The present model is directly derived from the modified R–P equation with bubble–bubble interactions. The only interaction coefficient that can be obtained is from the bubble cloud simulation.

In this section, the newly proposed model is further compared with the Kunz and Zwart cavitation models, where the empirical parameters from different sources are compared (see Table 2).

Three-dimensional cavitating flows are also simulated, where a cylinder with a hemispherical head (diameter $d = 25\ mm$) is applied (Rouse and Msnown, 1948). The numerical setup for this is shown in Fig. 7; the cylinder is mounted on an axis with $AOA = 0°$. The free-stream velocity $U_\infty = 5.37$ m/s, and the saturation pressure is set as 2300 Pa, with the outlet pressure adjusted to correspond to the cavitation number. A structured mesh is used in the model, with 1.6×10^6 cells, and the average of y^+ is 2 at the walls.

Fig. 8 shows the typical results from the numerical simulations, where the cavity distribution at $\sigma = 0.2$ is presented; it illustrates that the cavitation region can be divided into an attached cavitation subregion and a cloud cavitation region (Du et al., 2017). In the first region, $\alpha = 1.0$ and the cavity attaches to the wall stably. In the second region, α decreases and the cavity shrinks. The proposed

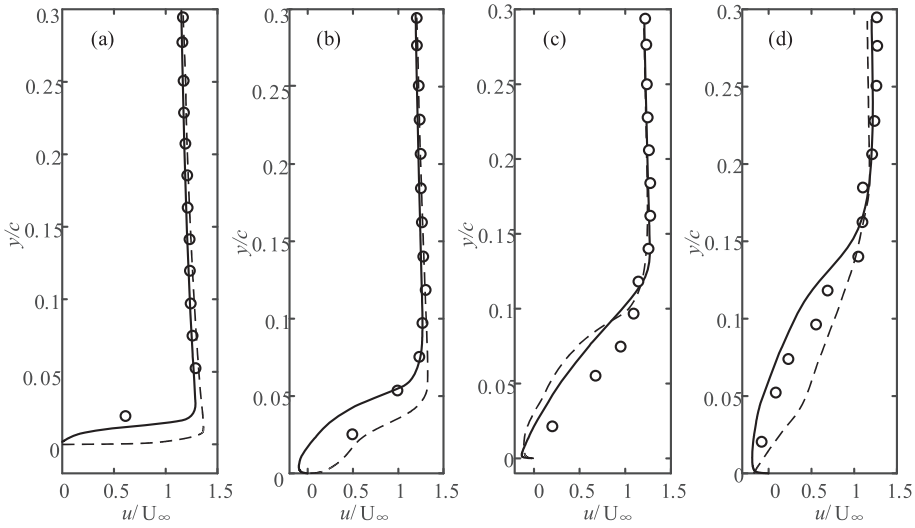

Fig. 6. Ensemble-averaged streamwise velocity profiles at four selected chordwise locations: $x/c = 0.2,\ 0.4,\ 0.6,$ *and* 0.8. The solid curves represent the results of the proposed cavitation model, and the dashed curves represent the results of the Kunz model. The open circles are from the experiments (Huang et al., 2013). In the figures, the velocity is normalized by the inlet velocity, U_∞.

Table 2
Adjustable empirical parameters for the cavitation models.

	Cavitation model	Adjustable parameters	
		C_v	C_c
K-1 (Morgut et al., 2011)	Kunz	4100	455
K-2, (Vaidyanathan et al., 2003)	Kunz	8×10^5	4×10^4
Z-1, (Geng and Escaler, 2019)	Zwart	300	0.08
Z-2, (Zwart et al., 2004)	Zwart	0.4	0.001
Present model		Physical determined, no needs for explicit given	

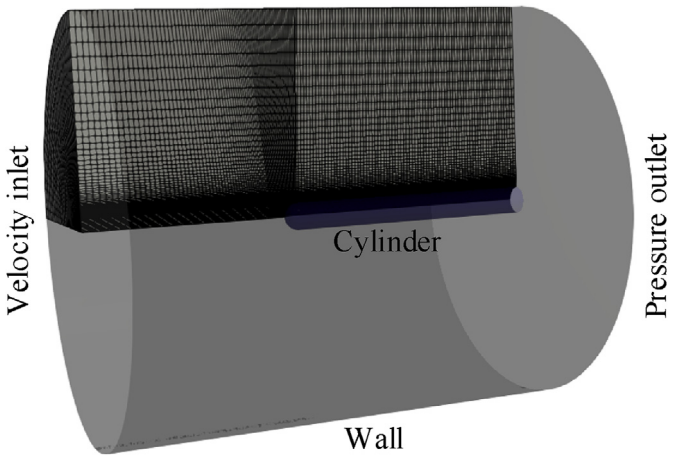

Fig. 7. Computational domain and mesh for simulation of the three-dimensional cavitating flow. A cylinder with a hemispherical head was used.

and traditional models provide similar predictions that are qualitatively good.

Then, the time-averaged pressure coefficients, C_p, are compared for the present, Zwart, and Kunz models. This coefficient is defined as

$$C_p = \frac{p - p_0}{0.5\rho U_\infty^2}, \tag{23}$$

where p is the local static pressure and p_0 is the reference pressure (Wang et al., 2001). Fig. 9 shows that the accuracies of the previous models depend on the empirical parameters. It should be noted that the K-1 and Z-1 parameters were optimized in the two-dimensional cavitating flow calculation (Morgut et al., 2011; Geng and Escaler, 2019), but they do not provide good predictions in the three-dimensional cases. Meanwhile, it is also shown that the empirical parameters are case-dependent: Z-1 predicts the flow, with $\sigma = 0.2$ being worse than $\sigma = 0.3$. However, the present model provides better predictions for both two- and three-dimensional simulations, and the parameter k was as evaluated previously in Section 3.1. Cavity breaks up into bubbles at the cavity closure, and bubbles collapse. The collapse velocity is signally affect by the bubble-bubble interaction. The pressure peak is significantly inhibited with present model at the cavity closure.

4. Conclusions

In the present work, a modified cavitation model is proposed by considering bubble–bubble interactions, second-order derivatives, and surface tension. The model is derived in the framework of the transport-equation-based approach, where the mass source term is modified. Using the inter-bubble actions, the governing equation describing bubble dynamics was solved carefully. The assumptions

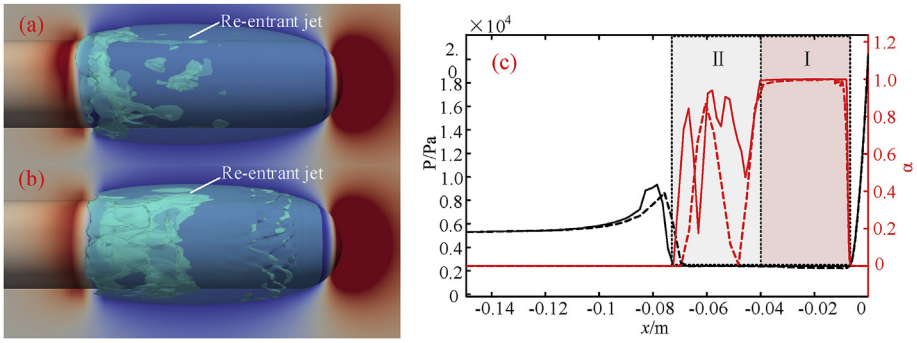

Fig. 8. Pressure distribution and cavity profile ($\alpha = 0.5$) on a cylinder for $\sigma = 0.2$ by (a) the proposed model and (b) K-1 model. (c) The solid and dashed curves show the results of the present and Kunz models, respectively. (Region I: attached cavitation, Region II: cloud cavitation).

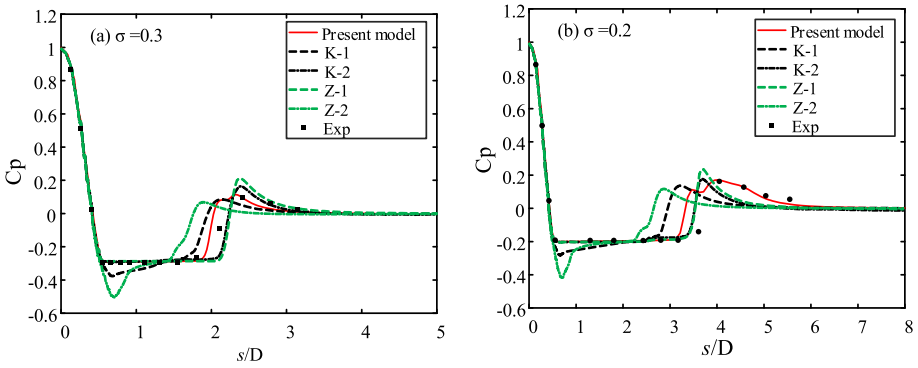

Fig. 9. Comparison of the time-averaged pressure coefficients over the cylinder for the simulations and experiments (Rouse and Msnown, 1948).

of identical spherical bubbles (in the cloud), fixed positions, and fixed bubble number were applied. Validation tests were then carried out, including the collapse of a bubble cloud as well as cavitating flows around a two-dimensional hydrofoil and three-dimensional cylinder with a hemispherical head. The significance of the current modifications for numerical performance includes the following:

- The modified model accurately predicts the collapsing velocity of the bubble cloud at the initial stage by considering the bubble–bubble interactions. At the last stage, the inertia effect, shown as the second-order derivative, plays a more important role and accelerates the collapse rate. These characteristics cannot be captured by the previous models, such as the Zwart model.
- Cavitation flows around a two-dimensional hydrofoil and three-dimensional cylinder were simulated. The modified cavitation model shows higher accuracy for cavitation prediction compared with the traditional model. The re-entry jets were obtained in both cases. More importantly, the only adjustable parameter in the proposed model is constant and independent of the case being considered.

The assumption of a constant bubble number limits the physical reality of this model, given that the bubbles could disintegrate or coalesce during cavitation (Du et al., 2016). Therefore, further improvements need to be made to the model, including criteria for nonsphericity and coalescence/disintegration of the bubbles.

Declaration of competing interest

The authors declare that they have no known competing financial interests or personal relationships that could have appeared to influence the work reported in this paper.

Acknowledgment

The authors gratefully acknowledge the support of the National Natural Science Foundation of China (Nos. 11872315, 51679202, and 51579209); the authors also wish to sincerely thank Prof. L. Zhang at ZJU for the fruitful discussions.

References

Bremond, N., Arora, M., Ohl, C.D., Lohse, D., 2006. Controlled multibubble surface cavitation. Phys. Rev. Lett. 96, 224501. https://doi.org/10.1103/PhysRevLett.96.224501.

Brennen, C.E., 1993. Cavitation and Bubble Dynamics. Oxford University Press, New York.

Chen, X.P., 2010. Simulation of 2D cavitation bubble growth under shear flow by lattice Boltzmann model. Commun. Comput. Phys. 7, 212–223. https://doi.org/10.4208/cicp.2009.09.015.

Delannoy, Y., Kueny, J.L., 1990. Two phase flow approach in unsteady cavitation modelling. ASME Cavitation Multiphase Flow Forum 98, 153–160.

Du, T.Z., Wang, Y., Liao, L.J., Huang, C.G., 2016. A numerical model for the evolution of internal structure of cavitation cloud. Phys. Fluids 28, 077103. https://doi.org/10.1063/1.4958885.

Du, T.Z., Wang, Y.W., Huang, C.G., Liao, L.J., 2017. A numerical model for cloud cavitation based on bubble cluster. Theor. Appl. Mech. Lett. 7, 231–234. https://doi.org/10.1016/j.taml.2017.08.001.

Geng, L., Escaler, X., 2019. Assessment of RANS turbulence models and Zwart cavitation model empirical coefficients for the simulation of unsteady cloud cavitation. Eng. Appl. Comput. Fluid Mech. 14, 151–167. https://doi.org/10.1080/19942060.2019.1694996.

Gevari, M.T., Abbasiasl, T., Niazi, S., et al., 2020. Direct and indirect thermal applications of hydrodynamic and acoustic cavitation: a review. Appl. Therm. Eng. 64, 104996. https://doi.org/10.1016/j.applthermaleng.2020.115065.

Goncalves, E., Patella, R.F., 2009. Numerical simulation of cavitating flows with homogeneous models. Comput. Fluids 38, 1682–1696. https://doi.org/10.1016/j.compfluid.2009.03.001.

Goncalves, E., 2011. Numerical study of unsteady turbulent cavitating flows. Eur. J. Mech. B Fluid 30, 26–40. https://doi.org/10.1016/j.euromechflu.2010.08.002.

Hirt, C.W., Nichols, B.D., 1981. Volume of fluid (VOF) method for the dynamics of free boundaries. J. Comput. Phys. 39, 201–225. https://doi.org/10.1016/0021-9991(81)90145-5.

Huang, B., Young, Y., Wang, G., Shyy, W., 2013. Combined experimental and computational investigation of unsteady structure of sheet/cloud cavitation. J. Fluid Eng. 135, 071301 https://doi.org/10.1115/1.4023650.

Ida, M., 2009. Multibubble cavitation inception. Phys. Fluids 21, 113302. https://doi.org/10.1063/1.3265547.

Kubota, A., Kato, H., Yamaguchi, H., 1992. A new modelling of cavitating flows: a numerical study of unsteady cavitation on a hydrofoil section. J. Fluid Mech. 240, 59–96. https://doi.org/10.1017/S002211209200003X.

Long, X., Cheng, H., Ji, B., Arndt, R.E., 2017. Numerical investigation of attached cavitation shedding dynamics around the Clark-Y hydrofoil with the FBDCM and an integral method. Ocean. Eng. 137, 247–261. https://doi.org/10.1016/j.oceaneng.2017.03.054.

Ma, J.S., Hsiao, C.T., Chahine, G.L., 2018. Numerical study of acoustically driven bubble cloud dynamics near a rigid wall. Ultrason. Sonochem. 40, 944–954. https://doi.org/10.1016/j.ultsonch.2017.08.033.

Maeda, K., Colonius, T., 2018. Eulerian–Lagrangian method for simulation of cloud cavitation. J. Comput. Phys. 371, 994–1017. https://doi.org/10.1016/j.jcp.2018.05.029.

Maiga, M.A., Coutier-Delgosha, O., Buisine, D., 2018. A new cavitation model based on bubble-bubble interactions. Phys. Fluids 30, 123301. https://doi.org/10.1063/1.5052257.

Maiga, M.A., Coutier-Delgosha, O., Buisine, D., 2019. Analysis of sheet cavitation with bubble/bubble interaction models. Phys. Fluids 31, 073302. https://doi.org/10.1063/1.5095781.

Menter, F.R., 1993. Zonal two equation k-ω turbulence models for aerodynamic flows. AIAA Paper 32, 1598–1605. https://doi.org/10.2514/3.12149.

Mettin, R., Akhatov, I., Parlitz, U., Ohl, C.D., 1993. Bjerknes forces between small cavitation bubbles in a strong acoustic field. Phys. Rev. E 56, 2924–2931. https://doi.org/10.1103/PhysRevE.56.2924.

Morgut, M., Nobile, E., Bilus, I., 2011. Comparison of mass transfer models for the numerical prediction of sheet cavitation around a hydrofoil. Int. J. Multiphas. Flow 37, 620–626. https://doi.org/10.1016/j.ijmultiphaseflow.2011.03.005.

Niederedzka, A., Schnerr, G.H., Sobieski, W., 2016. Review of numerical models of cavitating flows with the use of the homogeneous approach. Arch. Therm. 37, 71–88. https://doi.org/10.1515/aoter-2016-0013.

Peng, X., Wang, B., Li, H., Xu, L., Song, M., 2017. Generation of abnormal acoustic noise: singing of a cavitating tip vortex. Phys. Rev. Fluids 2, 053602. https://doi.org/10.1103/PhysRevFluids.2.053602.

Plesset, M.S., 1949. The dynamics of cavitation bubbles. J. Appl. Mech. 16, 228–231. https://resolver.caltech.edu/CaltechAUTHORS:20140808-114249321.

Rasthofer, U., Wermelinger, F., Karnakov, P., Šukys, J., Koumoutsakos, P., 2019. Computational study of the collapse of a cloud with 12500 gas bubbles in a liquid. Phys. Rev. Fluids 4, 063602. https://doi.org/10.1103/PhysRevFluids.4.063602.

Roohi, E., Zahiri, A.P., Passandideh-Fard, M., 2013. Numerical simulation of cavitation around a two-dimensional hydrofoil using VOF method and LES turbulence model. Appl. Math. Model. 37, 6469–6488. https://doi.org/10.1016/j.apm.2012.09.002.

Rouse, H., Msnown, J.S., 1948. Cavitation and Pressure Distribution, Head Forms at Zero Angle of Yaw. State University of Iowa, Iowa.

Sauer, J., Schnerr, G.H., 2001. Development of a new cavitation model based on bubble dynamics. J. Appl. Math. Mech. 81, 561–562. https://doi.org/10.1002/zamm.20010811559.

Singhal, A.K., Athavale, M.M., Li, H.Y., Jiang, Y., 2002. Mathematical basis and validation of the full cavitation model. J. Fluid Eng. 124, 617–624. https://doi.org/10.1115/1.1486223.

Stride, E., Segers, T., Lajoinie, G., 2020. Microbubble agents: new directions. Phys. Med. Biol. 46, 1326–1343. https://doi.org/10.1016/j.ultrasmedbio.2020.01.027.

Tiwari, T., Pantano, C., Freund, J.B., 2015. Growth-and-collapse dynamics of small bubble clusters near a wall. J. Fluid Mech. 775, 1–23. https://doi.org/10.1017/jfm.2015.287.

Vaidyanathan, R., Senocak, I., Wu, J., Shyy, W., 2003. Sensitivity evaluation of a transport-based turbulent cavitation model. J. Fluid Eng. 125, 447–458. https://doi.org/10.1115/1.1566048.

Wan, C., Wang, B., Wang, Q., et al., 2017. Probing and imaging of vapor–water mixture properties inside partial/cloud cavitating flows. J. Fluid Eng. 139, 031303 https://doi.org/10.1115/1.4035013.

Wang, G., Senocak, I., Shyy, W., 2001. Dynamics of attached turbulent cavitating flow. Prog. Aero. Sci. 37, 551–581. https://doi.org/10.1016/S0376-0421(01)

00014-8.
Wang, C.C., Wang, G.Y., Huang, B., 2020. Dynamics of unsteady compressible cavitating flows associated with the cavity shedding. Ocean. Eng. 209, 107025. https://doi.org/10.1016/j.oceaneng.2020.107025.
Ye, Y., Li, G., 2016. Modeling of hydrodynamic cavitating flows considering the bubble-bubble interaction. Int. J. Multiphas. Flow 84, 155–164. https://doi.org/10.1016/j.ijmultiphaseflow.2016.03.022.
Zhang, Y.N., Min, Q., Zhang, Y.N., Du, X.Z., 2016. Effects of liquid compressibility on bubble-bubble interactions between oscillating bubbles. J. Hydrodyn. B 28, 832–839. https://doi.org/10.1016/S1001-6058(16)60685-6.
Zhang, L.X., Zhang, J., Deng, J., 2019. Numerical investigation on the collapse of a bubble cluster near a solid wall. Phys. Rev. E 99, 043108. https://doi.org/10.1103/PhysRevE.99.043108.
Zwart, P.J., Gerber, A.G., Belamri, T., 2004. A two-phase flow model for predicting cavitation dynamics. Proc. Int. Conf. Multiphase Flow 152.